Reconstruction of cone-beam projections from Compton scattered data

Lucas C. Parra[1]

Abstract

The problem of reconstructing a 3D source distribution from Compton scattered data can be separated into two tasks. First, the angular distribution of line projections at different observation points within the detector volume are reconstructed. Then, reconstruction techniques are applied to the resulting cone-beam projections to synthesize the 3D source distribution. This paper describes an analytic solution for the first, yet unsolved, task. Building on the convolution theorem in spherical coordinates, a back-projection and inverse filtering technique in terms of spherical harmonics is formulated. The rotation invariance of the point response of the back-projection in spherical coordinates is proved; and the corresponding inverse filter function is derived. The resulting filtered back-projection algorithm then consists of a summation over all detected events of fixed and known event response functions. Measurement errors, which for Compton scatter detectors are typically different for each detected event, can easily be accounted for in the proposed algorithm. The computational cost of the algorithm is $O(NT^2)$, where N is the number of detected events and π/T is the desired angular resolution.

I. INTRODUCTION

The information collected in a Compton event includes the location where a primary γ-quantum is scattered, the energy transferred to a recoil electron, and the direction of the Compton scattered secondary γ-quantum. A scatter angle can be computed from the transferred energy; thus, for a given event, the origin of the primary quantum can be determined to lie somewhere on a cone-surface (see Figure 1).

Various approaches have been proposed to compute the generating 3D source distribution from a collection of scattered Compton events. A pioneer in the concept of the Compton camera, Singh, has presented a series of reconstruction methods mainly concerned with numerical methods like ML, EM, ART, etc. [1, 2]. These algorithms, in general, require binning of the data. However, due to the dimensionality of the measurement space (six dimensions) this may not be an optimal approach.

Analytic, rather than numeric solutions have also been proposed to solve the 3D source reconstruction problem [3, 4, 5]. In all instances, the problem is separated into two steps. First, cone-beam or plane projections of the source at different observations points within the detector volume are reconstructed from the measured data. Then synthesis techniques from the field of Computed Tomography are

applied to the resulting projections to generate the 3D source distribution. Cree and Bones [4] have developed an analytic expression for direct reconstruction, by severely limiting the accepted events to only those with secondary γ-quanta perpendicular to a detector array. Basko et al. [5] use spherical harmonics to convert cone-surface projections into plane projections; however, they ignore the dependency of the scatter likelihood on the scatter angles given by the Klein-Nishina distribution, and therefore fail to account for a crucial property of Compton scatter.

In this paper we suggest a similar two-step approach to the 3D source reconstruction problem. In the first step we use spherical harmonics to recover cone-beams from cone-surface projections. In contrast to [5], our method does not require costly decomposition into spherical harmonics during reconstruction. Instead, motivated by the work of Krzyzanowski [3], we use the deconvolution in spherical coordinates, to obtain a filtered back-projection technique which generates the cone-beam projections directly from the Compton scattered data. The inverse point-spread function in spherical harmonics, (referred to as the *event response function*) is fixed and can be computed prior to reconstruction. Our approach avoids Krzyzanowski's problem of a theoretically non-convergent angular reconstruction technique. To compute the 3D source distribution from the projections, we propose cone-beam reconstruction techniques [7, 8]; these are admittedly more complex than the simple Radon inversion used in [5]. Our algorithm goes beyond previous approaches in that it accounts for measurement errors which vary from event to event (an additional difficulty that arises for any real Compton scatter detectors).

II. MEASUREMENTS AND IMAGE GENERATION

Consider a particular volume element of a detector where Compton scattering events are being observed (see Figure 1). Our discussion throughout this paper will focus on such a single volume element in the detector. A particular direction from which primary γ-quanta originate can be described by the angles φ_1, (azimuth), and ϑ_1 (elevation). Using Ω_1 to denote the angle pair (φ_1, ϑ_1), the density of the γ-quanta detected from direction Ω_1 is denoted by $g(\Omega_1)$. Thus, $g(\Omega_1)$ gives the projection of the three dimensional source distribution along the line which intersects the volume element from direction Ω_1; i.e., $g(\Omega_1)$ gives the *cone-beam projections*. A Compton camera measures the directions Ω_2 of the scattered secondary γ-quanta. By also measuring the energy E_e of the recoil electron, the kinematics of Compton scattering gives us the scatter angle ω_2,

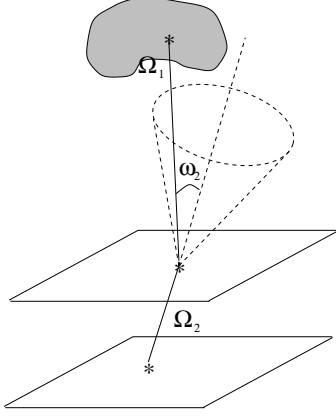$$\cos \omega_2 = 1 - \frac{E_e}{\gamma(h\nu - E_e)}, \tag{1}$$

Figure 1: Cone surface projection of a Compton scattering event. Positions indicated with an * represent locations of an emission of primary quantum, location of scatter, and detection of the secondary quantum. The orientations of the primary and secondary quanta are Ω_1 and Ω_2, respectively. The location of the scattering event, the absorption of the secondary quantum, and the scatter angle ω_2 can be measured, and together determine the origin point of the emission of the primary quantum to lie within the cone-surface shown.

where $\gamma = h\nu/m_e c^2$, $h\nu$ is the energy of the primary γ-quantum and $m_e c^2 = 511 keV$ [9]. The Compton camera therefore collects an image intensity distribution $f(\varphi_2, \vartheta_2, \omega_2)$ over three angles for every volume element in the detector.

To derive an analytic solution to the reconstruction problem, we must first derive an expression that describes how a measured image $f(\varphi_2, \vartheta_2, \omega_2)$ generates from a given angular distribution of line projections $g(\Omega_1)$. Let $p(\Omega_2, \omega_2 | \Omega_1)$ denote the probability density of making the observation Ω_2, ω_2, given that the event originated from direction Ω_1. We can then write:

$$f(\Omega_2, \omega_2) = \int d\Omega_1 p(\Omega_2, \omega_2 | \Omega_1) g(\Omega_1) . \qquad (2)$$

Denoting the angle $\angle \Omega_1 \Omega_2 = \omega$, we can write:

$$p(\Omega_2, \omega_2 | \Omega_1) = (2\pi)^{-1} \delta(\cos \omega_2 - \cos \omega) p(\omega) . \qquad (3)$$

The probability distribution $p(\omega)$ of measuring an event with scatter angle ω is proportional to the differential cross-section, $h(\cos \omega)$

$$p(\omega) \propto \frac{d\sigma}{d\Omega_2} \propto h(\cos \omega) ; \qquad (4)$$

and variations in detector efficiency as a function of scatter angle or position in detector volume (arising from detector architecture) can be accounted for in the definition of $h(\cos \omega)$.

Given $h(\cos \omega)$, Eq.(2) for image formation now becomes:

$$f(\Omega_2, \omega_2) = \int d\Omega_1 g(\Omega_1) h(\cos \omega) \delta(\cos \omega_2 - \cos \omega) . \qquad (5)$$

The proportionality factor $\left(2\pi \int d(\cos \omega) h(\cos \omega) \right)^{-1}$ can be absorbed into the definition of f or g. In order to reconstruct

for every point in the detector volume, the distribution of line projections $g(\Omega_1)$ from the measured data $f(\Omega_2, \omega_2)$, Eq.(5) must be inverted. Given $g(\Omega_1)$ for a manifold of scatter points, a cone-beam projection algorithm can then be used to recover the 3D source distribution.

III. SPHERICAL DECONVOLUTION

First consider the measured image intensity $f(\Omega_2, \omega_2)$ summed over all measured scatter angles ω_2:

$$f(\Omega_2) = \int d(cos \omega_2) f(\Omega_2, \omega_2). \qquad (6)$$

Applying this integration to Eq. (5) we obtain:

$$f(\Omega_2) = \int d\Omega_1 g(\Omega_1) h(\cos \omega) . \qquad (7)$$

This integration can be performed analytically by applying the following spherical trigonometry relation between Ω_1 and Ω_2:

$$\cos \omega = \cos \vartheta_1 \cos \vartheta_2 + \sin \vartheta_1 \sin \vartheta_2 cos(\varphi_1 - \varphi_2) . \qquad (8)$$

Eq.(7) can be interpreted as a convolution in the spherical coordinate space, with convolution kernel $h(\cos \omega)$. Since the convolution kernel depends only on the angular distance between Ω_1 and Ω_2, this integral equation is shift invariant in the angular space (rotationally invariant). Furthermore, it can be shown that, by expanding both sides of equation (7) in the appropriate system of orthogonal basis functions, the right side of Eq.(7) is transformed into a product. This is analogous to the convolution theorem in Cartesian coordinates .

In this context, the following deconvolution formula can be derived :

$$g(\Omega_1) = \int d\Omega_2 f(\Omega_2) h^{-1}(\cos \omega) , \qquad (9)$$

where

$$h^{-1}(\cos \omega) = \sum_{n=0}^{\infty} \left(\frac{2n+1}{4\pi} \right)^2 \frac{P_n(\cos \omega)}{H_n} , \qquad (10)$$

the expansion coefficients H_n are given by

$$H_n = \frac{2n+1}{2} \int d(\cos \omega) h(\cos \omega) P_n(\cos \omega), \qquad (11)$$

and the basis functions $P_n(\cos \omega)$ are Legendre polynomials. This deconvolution formula can be used to reconstruct the distribution of line projections $g(\Omega_1)$.

However, in employing Eq.(10), we encounter a difficulty typical in inverse filtering: the presence of the expansion coefficients H_n in the denominator. To avoid instability, these coefficients must be significantly different from zero. Unfortunately, as seen in Figure 2, the inverse of the convolution kernel corresponding to the differential cross-section of Compton scatter (cf. Eq. (23)) will have some

vanishing expansion coefficients. In fact, only the first few coefficients give finite values.

To solve this problem, inverse filtering techniques suggest generation of a summation image by back projection of the measured events. The summation image of the back-projections usually satisfies a linear convolution like that in Eq.(7). Once the overall transfer function from source to summation image has been computed, one can use inverse filtering according to Eqs. (9)-(11).
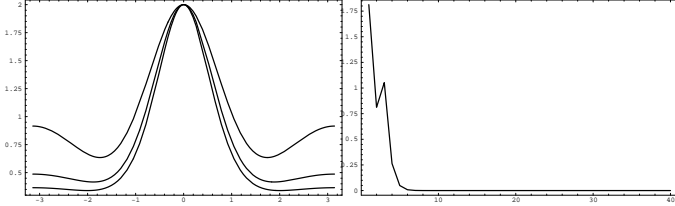

Figure 2: Left: differential cross section $h_c(\omega)$ of Compton scattering given in Eq. (23) for three primary quantum Energies $140keV$, $360keV$ and $511keV$. Right: First 40 corresponding expansion coefficients H_n^c in the base of Legendre polynomials, plotted only for $140keV$

IV. BACK-PROJECTION AND INVERSE FILTERING

The main problem confronted in the angular reconstruction is ambiguity in the event measurements. A particular event measured at coordinates Ω_2, ω_2 could have originated from any direction Ω_1, so long as Ω_1 forms an angle ω_2 with Ω_2. This set of possible directions form a cone-surface of ambiguity. *Back-projection* entails assigning to all directions Ω_1' which might have contributed to a particular $f(\Omega_2, \omega_2)$, the same image intensity: $f(\Omega_2, \omega_2)\delta(\cos\omega_2 - \cos\omega')$, where $\omega' = \angle\Omega_1'\Omega_2$.

One can then define a *summation image* $g'(\Omega_1')$ of the back-projections:

$$g'(\Omega_1') = \int d(\cos\omega_2) \int d\Omega_2 f(\Omega_2, \omega_2)\delta(\cos\omega_2 - \cos\omega').$$
(12)

This can be interpreted as summing intensities $f(\Omega_2, \omega_2)$ onto the unit sphere along circles with center Ω_2 and opening ω_2. We will now demonstrate that the resulting summation image can be expressed by an angular convolution of the line projections $g(\Omega_1)$ with an appropriate point spread function. This can then be used to reconstruct $g(\Omega_1)$ from $g'(\Omega_1')$ by means of the deconvolution of Eq.(9).

First we will calculate the overall response function for a point-like distribution in angular space, that is, the *point spread function* of the scatter plus back-projection. The original distribution of line projections is given by $g_{\Omega_1^*}(\Omega_1) = \delta(\cos\vartheta_1 - \cos\vartheta_1^*)\delta(\varphi_1 - \varphi^*)$. The index Ω_1^* denotes that this is a particular distribution corresponding to an angular point located at Ω_1^*. Inserting this into Eq.(5) one obtains the observable distribution $f_{\Omega_1^*}(\Omega_2, \omega_2)$ after some

algebra:

$$f_{\Omega_1^*}(\Omega_2, \omega_2) = \int d(\cos\vartheta_1)d\varphi_1\delta(\cos\vartheta_1 - \cos\vartheta_1^*)\delta(\varphi_1 - \varphi_1^*)$$
$$h(\cos\omega)\delta(\cos\omega - \cos\omega_2) \quad (13)$$
$$= h(\cos\omega^*)\delta(\cos\omega^* - \cos\omega_2), \quad (14)$$

where Eq.(8) for ω, and the analogous expression for $\omega^* = \angle\Omega_1^*\Omega_2$ have been used. Inserting this result into Eq.(12) one obtains the desired point spread function in the summation image:

$$g'_{\Omega_1^*}(\Omega_1') = \int d(\cos\omega_2) \int d\Omega_2 h(\cos\omega^*)$$
$$\delta(\cos\omega^* - \cos\omega_2)\delta(\cos\omega_2 - \cos\omega') \quad (15)$$
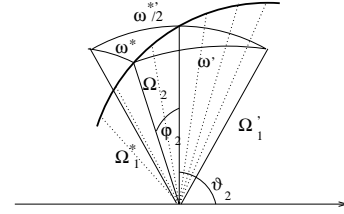$$= \int d\Omega_2 h(\cos\omega^*)\delta(\cos\omega^* - \cos\omega'). \quad (16)$$

Figure 3: The bold solid line shows the path along which the integration (with respect to Ω_2) for h_{bp} in Eq.(16) is performed.

Since the integral (16) must be calculated for a fixed set of angles Ω_1^*, Ω_1', we adapt the coordinate system for the integration parameters $\Omega_2 = \varphi_2, \vartheta_2$ as follows. Let the direction defined by $\vartheta_2 = \pi/2, \varphi_2 = 0$ divide the angle between Ω_1^* and Ω_1' as shown in Figure 3. For this choice of coordinate frame we have $\varphi^* = \varphi' = 0$, $\vartheta_1^* = \pi/2 + \omega'^*/2$ and $\vartheta_1' = \pi/2 - \omega'^*/2$. The δ-function in Eq.(16) limits the integration to a fixed $\vartheta_2 = \pi/2$ and arbitrary $\varphi_2 \in [0, 2\pi]$. Inserting this into the relations for $\cos\omega^*$ and $\cos\omega'$ in Eq.(8) we obtain:

$$\delta(\cos\omega^* - \cos\omega') = \delta(\cos\vartheta_2 2\sin\frac{\omega'^*}{2}) = \frac{1}{2\sin\frac{\omega'^*}{2}}\delta(\cos\vartheta_2).$$

Now integration over ϑ_2 can be performed easily:

$$g'_{\Omega_1^*}(\Omega_1') = \int d(\cos\vartheta_2)d\varphi_2 h(\cos\omega^*)\frac{\delta(\cos\vartheta_2)}{2\sin\frac{\omega'^*}{2}} \quad (17)$$

$$= \frac{1}{2\sin\frac{\omega'^*}{2}} \int_0^{2\pi} d\varphi_2 h(\sin\vartheta^* \cos(\varphi_1^* - \varphi_2)) \quad (18)$$

$$= \frac{1}{\sqrt{1 - \cos^2\frac{\omega'^*}{2}}} \int_{-\cos\frac{\omega'^*}{2}}^{\cos\frac{\omega'^*}{2}} dz \frac{h(z)}{\sqrt{\cos^2\frac{\omega'^*}{2} - z^2}} \quad (19)$$

$$= h_{bp}(\cos\omega'^*). \quad (20)$$

Note that the integration above produces a point spread function $h_{bp}(\cos\omega'^*)$ which depends only on the angle $\omega'^* = \angle\Omega_1'\Omega_1^*$ between the orientation of the angular point

source Ω_1^* and the observation point Ω_1' in the summation image; $h_{bp}(\cos \omega'^*)$ is shift invariant in the angular space. The summation image point spread function is shown in Figure 4.

An arbitrary source distribution $g(\Omega_1)$ can be understood as a linear superposition of point sources located at Ω_1 and weighting $g(\Omega_1)$. A point source generates in the summation image the point spread function $h_{bp}(\cos \omega_1)$, where $\omega_1 = \angle \Omega_1 \Omega_1'$. The summation image of the distribution $g(\Omega_1)$ is then a linear superposition of point spread function $h_{bp}(\cos \omega_1)$ with weighting $g(\Omega_1)$:

$$g'(\Omega_1') = \int d\Omega_1 g(\Omega_1) h_{\mathrm{bp}}(\cos \omega_1), \qquad (21)$$

This is now a convolution of the form of Eq.(7), and can be inverted by the deconvolution described in Eqs. (9)-(11) as follows:

$$g(\Omega_1) = \int d\Omega_1' g'(\Omega_1') h_{\mathrm{bp}}^{-1}(\cos \omega_1). \qquad (22)$$

The corresponding expansion coefficients H_n^{bp} of the Legendre polynomial decomposition can be calculated numerically, at fairly low computational cost, since they need to be calculated only once.
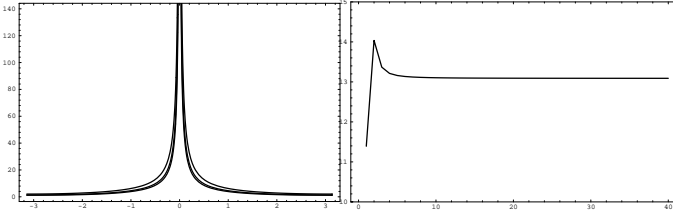

Figure 4: Left: Point spread function h_{bp} in the angular summation image for three different primary quantum Energies $140 keV$, $360 keV$ and $520 keV$. Right: First 40 expansion coefficients H_n^{bp} in the base of Legendre polynomials, plotted only for $140 keV$. With this coefficients the deconvolution kernel h_{bp}^{-1} for the inverse filtering can be calculated.

For unrestricted Compton scatter, the differential cross-section $h(\cos \omega)$ convolution kernel of Eq.(17) is given by the Klein-Nishina distribution [9] (shown in Figure 2):

$$h(\cos \omega) = h_{\mathrm{c}}(\cos \omega) \frac{1 + \cos^2 \omega + \frac{\gamma^2 (1 - \cos \omega)^2}{1 + \gamma(1 - \cos \omega)}}{(1 + \gamma(1 - \cos \omega))^2}, \qquad (23)$$

Surprisingly, even for this complex form for $h(\cos \omega)$, the resulting integral can be computed in closed form; however, for simplicity, this computation will be omitted here. In Figure 4 it can be seen that for the Compton scatter the H_n^{bp} converge after a few coefficients to a constant value. Fortunately, now they are non-zero and the convolution in Eq. (21) can easily be inverted using the deconvolution kernel defined as in Eq. (10). Given a convolution kernel $h(\cos \omega)$ chosen to account for detector geometry and sensitivity, the integral in Eq.(17) can be computed numerically. This computation could be performed once off-line, before reconstruction.

V. FILTERED BACK-PROJECTION

The procedure described in the previous section for reconstructing cone-beam projections from Compton cone-surface projections consists of generation of a summation image, followed by deconvolution. The deconvolution can be performed either directly in the angular space, or by transforming into the spherical harmonics domain, then filtering, then inverse transforming.

It is possible, however, to combine the back-projection of Eq.(12) and the deconvolution of Eq.(22) into the following single filtered back-projection step as follows:

$$g(\Omega_1) = \int d\Omega_1' g'(\Omega_1') h_{\mathrm{bp}}^{-1}(\cos \omega_1) \qquad (24)$$

$$= \int d\Omega_1' \int d(\cos \omega_2) \int d\Omega_2 f(\Omega_2, \omega_2)$$
$$\delta(\cos \omega_2 - \cos \omega') h_{\mathrm{bp}}^{-1}(\cos \omega_1) \qquad (25)$$

$$= \int d(\cos \omega_2) \int d\Omega_2 f(\Omega_2, \omega_2) \int d\Omega_1'$$
$$\delta(\cos \omega_2 - \cos \omega')$$
$$h_{\mathrm{bp}}^{-1}(\cos \vartheta_1 \cos \vartheta_1' + \sin \vartheta_1 \sin \vartheta_1' \cos(\varphi_1 - \varphi_1'))$$
$$\qquad (26)$$

$$= \int d(\cos \omega_2) \int d\Omega_2 f(\Omega_2, \omega_2) \int d\varphi_1'$$
$$h_{\mathrm{bp}}^{-1}(\cos \omega \cos \omega_2 + \sin \omega \sin \omega_2 \cos(\varphi_1 - \varphi_1'))$$

$$= \int d(\cos \omega_2) \int d\Omega_2 f(\Omega_2, \omega_2) R(\omega, \omega_2). \qquad (27)$$

For the integration over ϑ_1' on line (26), the z-axis has been chosen to point in the Ω_2 direction. Then $\vartheta_1 = \omega$, $\vartheta_1' = \omega'$, and integration of the δ-function replaces ω' by ω_2. We refer to function $R(\omega, \omega_2)$ as the *event response* of a Compton event.

The integration in $R(\omega, \omega_2)$ over φ_1' can be performed analytically as follows:

$$R(\omega, \omega_2)$$
$$= \int d\varphi_1' h_{\mathrm{bp}}^{-1}(\cos \omega \cos \omega_2 + \sin \omega \sin \omega_2 \cos(\varphi_1 - \varphi_1'))$$
$$= \sum_{n=0}^{\infty} \left(\frac{2n+1}{4\pi}\right)^2 \frac{1}{H_n^{\mathrm{bp}}}$$
$$\int d\varphi_1' P_n(\cos \omega \cos \omega_2 + \sin \omega \sin \omega_2 \cos(\varphi_1 - \varphi_1'))$$
$$= \sum_{n=0}^{\infty} \left(\frac{2n+1}{4\pi}\right)^2 \frac{2\pi}{H_n^{\mathrm{bp}}} P_n(\cos \omega_2) P_n(\cos \omega). \qquad (28)$$

An expansion of the Legendre polynomials in terms of spherical harmonics and the integration leading to line (28) uses the definition of spherical harmonics. For a measured distribution having bandwidth T, the summation over n can be truncated at T.

In practice, image intensity $f(\Omega_2, \omega_2)$ will be measured at a set of N data points: $(\varphi_2^1, \vartheta_2^1, \omega_2^1), ..., (\varphi_2^N, \vartheta_2^N, \omega_2^N)$.
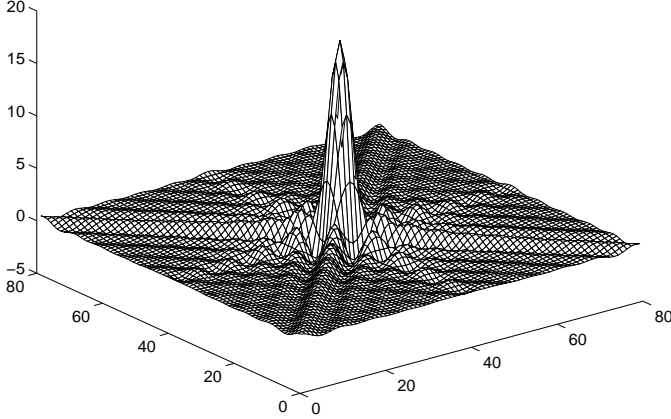
Figure 5: The event response function $R(\omega, \omega_2)$, calculated with expansion coefficients H_n^{bp}, for primary quantum energy $140 keV$. The expansion has been truncated at order 20. The angles ω and ω_2 vary from $-\pi/2$ to $\pi/2$ along the horizontal plane.

The image intensity can therefore be expressed as a sum of δ-functions at the measurement points: $f(\Omega_2, \omega_2) = \sum_\nu \delta(\varphi_2 - \varphi_2^\nu)\delta(\cos\vartheta_2 - \cos\vartheta_2^\nu)\delta(\cos\omega_2 - \cos\omega_2^\nu)$.

Substituting this expression for $f(\Omega_2, \omega_2)$ into Eq.(27), we obtain for the reconstructed cone beam projection $g(\Omega_1)$:

$$g(\Omega_1) = \int d(\cos\omega_2) \int d\Omega_2 f(\Omega_2, \omega_2) R(\omega, \omega_2) \qquad (29)$$

$$= \sum_{\nu=1}^{N} R(\omega^\nu, \omega_2^\nu). \qquad (30)$$

Finally, we assign each event a response function on the angular space Ω_1, parameterized by the measured scatter angle ω_2. Summing these response functions for each event yields the filtered back-projection reconstruction.

In practice the angular resolution π/T is limited by measurement error. Therefore, it is reasonable to truncate the sum in Eq.(28) at $n = T$; and thus in the reconstruction of Eq.(30), only $2T$ bins are needed for each of the angles ϑ_1, and φ_1. As a result, the overall computational cost is $O(NT^2)$, if the event response function has been computed prior to reconstruction.

A serious complication in practical implementations of Compton scattering detectors is that every measured event can have associated with it a different measurement error. The accuracy with which the scatter angle ω_2 can be determined in general depends on the absolute value of the energy ΔE_e of the recoil electron; and furthermore, the precision of Ω_2 depends on the distance of scatter location and absorption.

The filtered back-projection procedure we have proposed in this section has considerable advantages with regards to these difficulties. In the back-projection and filtering technique outlined in the previous section, only *fixed* measurement errors can be considered. In contrast, with the technique described in this section we are free to use different event response functions for every event, with different coefficients H_n^{bp} computed for different measurement errors.

VI. Summary

An analytic technique for reconstruction of cone-beam projections from cone-surface projections has been derived. This linear procedure is applicable to an idealized detector, where the distribution of detected scatter angles is independent of the orientation of the incident primary γ-quantum. The proposed technique goes beyond previous analytic approaches also in that it may account for measurement errors which vary from event to event (a typical feature of real Compton scatter detectors).

A filtered back-projection procedure is used for reconstruction. With this procedure, every volume element in the detector is assigned a two dimensional angular space. For every scattering event in a particular volume element, an event response function is added in the angular space of the volume element. These summed response functions yield the cone-beam projections of the three dimensional source on that volume element.

VII. References

[1] Manbir Singh, "An electronically collimated gamma camera for single photon emission computed tomography. Part 1: Theoretical considerations and design criteria", *Medical Physics*, vol. 10, no. 4, pp. 421–427, 1983.

[2] Tom Hebert, Richard Leahy, and Manbir Singh, "Three-dimensional maximum-likelihood reconstruction for an electronically collimated single-photon-emission imaging system", *Optical Society of America*, vol. 7, no. 7, pp. 1305–1313, 1990.

[3] Waclaw Krzyzanowski, "Compton Lens Formula, A New way of recunstructing single-gamma emission images", Tech. Rep. Si-85-16, Physics Department, Siegen University, Siegen, Germany, 1985.

[4] J. Cree, Michael and J. Bones, Philip, "Towards Direct Reconstruction from Gamma Camera Based on Compton Scattering", *IEEE Transaction on Medical Imaging*, vol. 13, no. 2, pp. 398–407, 1994.

[5] R. Basko, G. Zeng, and G. Gullberg, "Application of spherical harmonics to image reconstruction for the Compton camera", *Phys. Med. Biol.*, vol. 43, pp. 887–894, 1998.

[6] S. Schaller, T. Flohr, and P. Steffen, "An efficient Fourier method for 3-D Radon inversion in exact cone-beam CT reconstruction", *IEEE Trans. on Medical Imaging*, vol. 17, no. 2, pp. 244–250, Apr. 1998.

[7] K.C. Tam, S. Samarasekera, and F. Sauer, "Exact cone beam CT with a spiral scan", *Physics in Medicine and Biology*, vol. 43, no. 4, pp. 1015–1024, Apr. 1998.

[8] Harrison Barrett and William Swindell, *Radiological Imaging*, vol. I and II, Academic Press, 1981.